Research Article

Modeling individual mobility's impact on COVID-19 transmission: Insights from a two-patch SEIR-V approach

M. Bouziane* , M.A. Boubekeur, , M.E.B. Keddar, and O. Belhamiti,

———————————

*Corresponding author

Mehdi Bouziane

Department of Mathematics, Higher Normal School of Mostaganem, Mostaganem 27000, Algeria. e-mail: mehdi.bouziane@univ-mosta.dz

Maroua Amel Boubekeur

Department of Mathematics and Computer Science,

Abdelhamid Ben Badis University, Mostaganem 27000, Algeria. e-mail: maroua.boubekeur.etu@univ-mosta.dz

Meriem El Batoul Keddar

Department of Mathematics and Computer Science,

Abdelhamid Ben Badis University, Mostaganem 27000, Algeria. e-mail: batoulkeddar@gmail.com

Omar Belhamiti

Department of Mathematics and Computer Science,

Abdelhamid Ben Badis University, Mostaganem 27000, Algeria. e-mail: omar.belhamiti@univ-mosta.dz

How to cite this article

Bouziane, M., Boubekeur, M.A., Keddar, M.E.B. and Belhamiti, O., Modeling individual mobility's impact on COVID-19 transmission: Insights from a two-patch SEIR-V approach. *Iran. J. Numer. Anal. Optim.*, 2024; 14(2): 580-612. https://doi.org/10.22067/ijnao.2024.85987.1365

Abstract

This research explores the influence of individual mobility on COVID-19 transmission, utilizing a temporal mathematical model to clarify disease spread and vaccination dynamics across diverse regions. Employing a computationally efficient two-patch configuration that emphasizes regional interactions, our study aims to guide optimal disease control strategies. The introduced SEIR-V model with a two-patch setup estimates the vaccination reproduction number, R_v, while equilibrium points and system stability are identified. Visualizations from numerical simulations and sensitivity analyses illustrate key parameters affecting the vaccination reproduction number and COVID-19 control measures. Our findings underscore system responsiveness, emphasizing the intricate relationship between R_v, migration rates, and disease prevalence.

1 Introduction

In December 2019, a coronavirus emerged in Wuhan, China, transmitted from animals to humans [22]. The outbreak escalated rapidly, with 44 reported cases in China by January 3, 2020 [29]. The virus swiftly spread nationwide, prompting the declaration of a state of epidemic in March 2020, exacerbated by global human migration and travel between cities [18, 20]. The facilitation of worldwide travel and commerce contributed to the rapid global dissemination, resulting in over 585 million reported cases and 6.4 million reported deaths as of August 2022 [28]. Consequently, a multitude of researchers have been captivated by the dynamics of COVID-19 dissemination [16, 6, 7, 9, 12].

The investigation focused on the movement patterns of individuals across a network during the global spread of COVID-19 in 203 countries [13]. Researchers observed that human mobility, particularly through cities and tourism, significantly contributed to the virus's dissemination, supported by Arino and others who affirmed that epidemic spread increases during trans-

portation [2]. Numerous epidemiologists, including Baister et al. [4], Ahmad et al. [1], McCarthy et al. [21], and Iyaniwura et al. [15] employed metapopulation models to explore COVID-19 transmission dynamics. These models considered diverse scenarios, such as studying individual mobility and social interactions in major cities, investigating vaccination strategies in a prison setting, and using hybrid gravity-metapopulation modeling to analyze the spread between different regions. Other studies delved into specific regions like Ireland and formulated generalized n-patch SEIR epidemiological models to devise effective control strategies against the disease [14, 19].

This paper introduces metapopulation modeling to investigate the impact of individual mobility on the spread of COVID-19, building upon our previous model [7]. Our focus is on developing a temporal mathematical model to describe COVID-19 transmission with vaccination, aiming to optimize disease control strategies within and between different regions. Using a two-patch configuration ($n = 2$), we address the complexities of calculations, ensuring the boundedness and positivity of solutions. We calculate the vaccination reproduction number (R_v) for the two-patch metapopulation and analyze the local and global stability of the disease-free equilibrium (DFE), establishing that if $R_v > 1$, then the disease becomes endemic. Sensitivity analysis and numerical simulations further explore the impact of key parameters on Rv, confirming the existence and stability of the endemic equilibrium. Additionally, we examine the influence of migration rates on COVID-19 transmission between the two patches.

The paper's structure unfolds as follows: Section 2 revisits the previously introduced and analyzed model. In Section 3, we introduce the metapopulation model. Section 4 proposes the SEIR-V model with a two-patch configuration for COVID-19, estimating the vaccination reproduction number (R_v). We identify equilibrium points and conduct stability analysis for the dynamic system of COVID-19 propagation. Section 5 presents numerical simulations and sensitivity analyses to illustrate theoretical results. Finally, Section 6 encapsulates our conclusions.

2 Baseline model

We first recall the model introduced and analyzed in [7], which describes the transmission dynamics of COVID-19. In this model, the population is subdivided into seven distinct groups: susceptible individuals (S), exposed but not yet infectious individuals (E), vaccinated individuals (V), asymptomatic infectious individuals (I_a), symptomatic and hospitalized infectious individuals (I_s), individuals who have succumbed to the disease (D), and those who have recovered (R).

It is assumed that there is no vertical transmission of the disease so that all births occur into the susceptible human class, at the rate $\mu > 0$. Moreover, we assume that the total human population N remains constant; thus, birth and death rates are equal.

Hence, the normalized reduced system is given by

$$
\begin{cases}
S'(t) = \mu - (\alpha_1 \eta + \alpha_2 (1 - \eta)) S(t) (I_a(t) + I_s(t)) - \mu S(t) \\
\qquad + \lambda_2 V(t) + \gamma R(t) - \lambda_1 S(t), \\
E'(t) = (\alpha_1 \eta + \alpha_2 (1 - \eta)) S(t) (I_a(t) + I_s(t)) - (\beta_1 + \beta_2 + \mu + \lambda_3) E(t), \\
V'(t) = \lambda_1 S(t) + \lambda_3 E(t) + \lambda_4 I_a(t) - (\lambda_2 + \lambda_5 + \mu) V(t), \\
I_a'(t) = \beta_1 E(t) - (\gamma_1 + \lambda_4 + \mu) I_a(t), \\
I_s'(t) = \beta_2 E(t) - (\gamma_2 + \delta + \mu) I_s(t), \\
R'(t) = \gamma_1 I_a(t) + \gamma_2 I_s(t) + \lambda_5 V(t) - \gamma R(t) - \mu R(t),
\end{cases}
\tag{1}
$$

where

α_1 is the infection rate of confined susceptible and α_2 is the infection rate of unconfined susceptible such as $\alpha_1 < \alpha_2$.

η is the confinement rate within the population.

$(\beta_i)_{i=1,2}$ are infected-infectious rates.

γ is the reinfection rate after recovery from a first infection.

$(\gamma_i)_{i=1,2}$ are the recovery rates.

$(\lambda_i)_{i=1,3,4}$ are the vaccination rates.

λ_2 is the rate of vaccine ineffectiveness.

λ_5 is the vaccine effectiveness rate.

δ is the COVID-19 mortality rate.

μ is the natality rate.

The study of the model is detailed in [7]. For this model (1), the vaccination reproduction number is given by

$$
R_v = \frac{(\alpha_1\eta + \alpha_2(1-\eta))}{(\gamma_1 + \lambda_4 + \mu)(\gamma_2 + \delta + \mu)} \tag{2}
$$
$$
\times \frac{(\beta_1(\gamma_2 + \delta + \mu) + \beta_2(\gamma_1 + \lambda_4 + \mu))(\lambda_2 + \lambda_5 + \mu)(\gamma + \mu)}{(\beta_1 + \beta_2 + \mu + \lambda_3)((\lambda_2 + \lambda_5 + \mu)(\gamma + \mu) + \lambda_1(\gamma + \lambda_5 + \mu))}.
$$

3 Metapopulation model

In works [4, 1, 21, 15, 14, 2, 19, 3], a comprehensive system of differential equations is developed to characterize human mobility. Within this model, subpopulations are identified based on their origin and their current location. Building upon the model detailed in the preceding section, we expand it by introducing the concept of a neighborhood wherein interactions occur between infected and non-infected individuals.

Consider a network comprising p nodes. Within this network, individuals are characterized by two key attributes: the node of origin, signifying their residence, and the node they currently occupy at time t. We assume that the total human population N_i in each node remains constant and strictly positive, and the transition rates from one pathological state to another also remain the same for all patches. Furthermore, we suppose that birth occurs in the resident node while deaths take place in any node where the human is present.

The population in the patch i, is divided into compartments of susceptible (S_i), exposed (E_i), vaccinated(V_i), asymptomatic infectious $(I_{a,i})$, symptomatic and hospitalized infectious $(I_{s,i})$, death (D_i), and the recovered as (R_i).

The total number of individuals in the patch i size at time t is defined by

$$
N_i = S_i(t) + E_i(t) + V_i(t) + I_{a,i}(t) + I_{s,i}(t) + R_i(t) + D_i(t),
$$

and the total population is given by

$$N = \sum_{i=1}^{p} N_i.$$

We adopt a methodology akin to that employed by Arino and van Den Driessche [3]. Migration is observed between any pair of patches, transpiring at the specified rates:

- φ_{ij}^{S} migration rate of susceptible individuals from the patch i to the patch j,

- φ_{ij}^{E} migration rate of infected individuals (noninfectious) from the patch i to the patch j,

- φ_{ij}^{V} migration rate of vaccination individuals from the patch i to the patch j,

- $\varphi_{ij}^{I_a}$ migration rate of asymptomatic infectious individuals from the patch i to the patch j,

- $\varphi_{ij}^{I_s}$ migration rate of symptomatic infectious individuals from the patch i to the patch j,

- φ_{ij}^{R} migration rate of recovered and immunized infectious individuals from the patch i to the patch j,

where

$$\varphi_{ii}^{S} = \varphi_{ii}^{E} = \varphi_{ii}^{V} = \varphi_{ii}^{I_a} = \varphi_{ii}^{I_s} = \varphi_{ii}^{R} = 0.$$

Hence, the metapopulation system of differential equations that will model the dynamics of coronavirus spread is the system given by

$$\begin{cases} \dfrac{dS_i}{dt} = \mu \dfrac{N_i}{N} - (\alpha_1 \eta_i + \alpha_2 (1 - \eta_i)) (I_{a,i} + I_{s,i}) S_i + \sum_{j=1(j \neq i)}^{p} \varphi_{ji}^{S} S_j \\ \qquad - \left(\sum_{j=1(j \neq i)}^{p} \varphi_{ij}^{S} \right) S_i - (\mu + \lambda_1) S_i + \lambda_2 V_i + \gamma R_i, \\ \dfrac{dE_i}{dt} = (\alpha_1 \eta_i + \alpha_2 (1 - \eta_i)) (I_{a,i} + I_{s,i}) S_i + \sum_{j=1(j \neq i)}^{p} \varphi_{ji}^{E} E_j \\ \qquad - \left(\sum_{j=1(j \neq i)}^{p} \varphi_{ij}^{E} \right) E_i - (\beta_1 + \beta_2 + \mu + \lambda_3) E_i, \\ \dfrac{dV_i}{dt} = \lambda_1 S_i + \lambda_3 E_i + \lambda_4 I_{a,i} + \sum_{j=1(j \neq i)}^{p} \varphi_{ji}^{V} V_j \\ \qquad - \left(\sum_{j=1(j \neq i)}^{p} \varphi_{ij}^{V} \right) V_i - (\lambda_2 + \lambda_5 + \mu) V_i, \\ \dfrac{dI_{a,i}}{dt} = \beta_1 E_i + \sum_{j=1(j \neq i)}^{p} \varphi_{ji}^{I_a} I_{a,j} - \left(\sum_{j=1(j \neq i)}^{p} \varphi_{ij}^{I_a} \right) I_{a,i} - (\gamma_1 + \lambda_4 + \mu) I_{a,i}, \\ \dfrac{dI_{s,i}}{dt} = \beta_2 E_i - (\gamma_2 + \delta + \mu) I_{s,i}, \\ \dfrac{dR_i}{dt} = \gamma_1 I_{a,i} + \gamma_2 I_{s,i} + \lambda_5 V_i + \sum_{j=1(j \neq i)}^{p} \varphi_{ji}^{R} R_j \\ \qquad - \left(\sum_{j=1(j \neq i)}^{p} \varphi_{ij}^{R} \right) R_i - (\gamma + \mu) R_i, \\ \dfrac{dD_i}{dt} = \delta I_{s,i}, \end{cases}$$

with initial conditions

$$\begin{cases} S_i(0) > 0, & E_i(0) \geqslant 0, & \sum_{i=1}^{p} E_i(0) > 0, \\ V_i(0) > 0, & I_{a,i}(0) \geqslant 0, & \sum_{i=1}^{p} I_{a,i}(0) > 0, \\ I_{s,i}(0) \geqslant 0, & \sum_{i=1}^{p} I_{s,i}(0) > 0, & R_i(0) > 0, \end{cases}$$

for $i = \overline{1, p}$.

4 Two-patch SEIR-V model for COVID-19

To enhance the realism of our study, we confine our investigation to a two-patch model, undertaking a rigorous mathematical analysis of its dynamics.

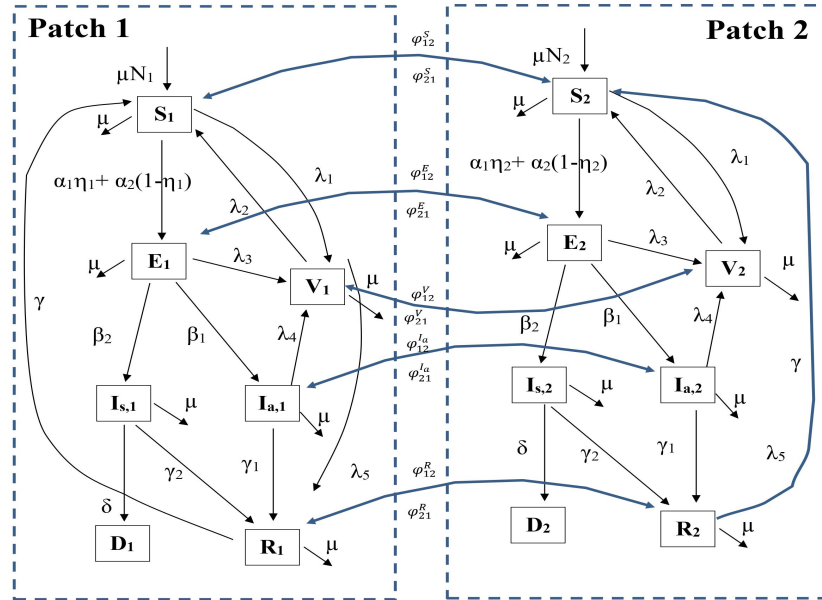The diagram of the transmission of COVID-19 in two-patch is shown in Figure 1.

Figure 1: Diagram of the proposed two-Patch SEIR-V Model.

The SEIR-V two-Patch model is formulated as follows:

$$\begin{cases} \dfrac{dS_1}{dt} = \mu n_1 - c_1 \left(I_{a,1} + I_{s,1}\right) S_1 + \varphi_{21}^S S_2 - \left(\varphi_{12}^S + c_0\right) S_1 + \lambda_2 V_1 + \gamma R_1, \\[2mm] \dfrac{dS_2}{dt} = \mu n_2 - c_2 \left(I_{a,2} + I_{s,2}\right) S_2 + \varphi_{12}^S S_1 - \left(\varphi_{21}^S + c_0\right) S_2 + \lambda_2 V_2 + \gamma R_2, \\[2mm] \dfrac{dE_1}{dt} = c_1 \left(I_{a,1} + I_{s,1}\right) S_1 + \varphi_{21}^E E_2 - \left(\varphi_{12}^E + c_3\right) E_1, \\[2mm] \dfrac{dE_2}{dt} = c_2 \left(I_{a,2} + I_{s,2}\right) S_2 + \varphi_{12}^E E_1 - \left(\varphi_{21}^E + c_3\right) E_2, \\[2mm] \dfrac{dV_1}{dt} = \lambda_1 S_1 + \lambda_3 E_1 + \lambda_4 I_{a,1} + \varphi_{21}^V V_2 - \left(\varphi_{12}^V + c_4\right) V_1, \\[2mm] \dfrac{dV_2}{dt} = \lambda_1 S_2 + \lambda_3 E_2 + \lambda_4 I_{a,2} + \varphi_{12}^V V_1 - \left(\varphi_{21}^V + c_4\right) V_2, \\[2mm] \dfrac{dI_{a,1}}{dt} = \beta_1 E_1 + \varphi_{21}^{I_a} I_{a,2} - \left(\varphi_{12}^{I_a} + c_5\right) I_{a,1}, \\[2mm] \dfrac{dI_{a,2}}{dt} = \beta_1 E_2 + \varphi_{12}^{I_a} I_{a,1} - \left(\varphi_{21}^{I_a} + c_5\right) I_{a,2}, \\[2mm] \dfrac{dI_{s,1}}{dt} = \beta_2 E_1 - c_6 I_{s,1}, \\[2mm] \dfrac{dI_{s,2}}{dt} = \beta_2 E_2 - c_6 I_{s,2}, \\[2mm] \dfrac{dR_1}{dt} = \gamma_1 I_{a,1} + \gamma_2 I_{s,1} + \lambda_5 V_1 + \varphi_{21}^R R_2 - \left(\varphi_{12}^R + c_7\right) R_1, \\[2mm] \dfrac{dR_2}{dt} = \gamma_1 I_{a,2} + \gamma_2 I_{s,2} + \lambda_5 V_2 + \varphi_{12}^R R_1 - \left(\varphi_{21}^R + c_7\right) R_2, \end{cases} \tag{3}$$

with initial conditions

$$\begin{cases} S_i(0) > 0, \\ E_i(0) \geqslant 0, \ E_1(0) + E_2(0) > 0, \\ V_i(0) > 0, \\ I_{a,i}(0) \geqslant 0, \ I_{a,1}(0) + I_{a,2}(0) > 0, \\ I_{s,i}(0) \geqslant 0, \ I_{s,1}(0) + I_{s,2}(0) > 0, \\ R_i(0) > 0, \end{cases} \tag{4}$$

for $i = \overline{1,2}$. Here

$$
\begin{cases}
n_1 = \frac{N_1}{N}, n_2 = \frac{N_2}{N}, \\
c_0 = (\mu + \lambda_1), \\
c_1 = (\alpha_1 \eta_1 + \alpha_2 (1 - \eta_1)), \\
c_2 = (\alpha_1 \eta_2 + \alpha_2 (1 - \eta_2)), \\
c_3 = \beta_1 + \beta_2 + \mu + \lambda_3,
\end{cases}
\quad
\begin{cases}
c_4 = (\lambda_2 + \lambda_5 + \mu), \\
c_5 = \gamma_1 + \lambda_4 + \mu, \\
c_6 = \gamma_2 + \delta + \mu, \\
c_7 = (\gamma + \mu).
\end{cases}
\tag{5}
$$

4.1 Boundedness and positivity of solutions

We consider the following zone of biological interest:

$$
\Omega = \Big\{ (S_1, S_2, E_1, E_2, V_1, V_2, I_{a,1}, I_{a,2}, I_{s,1}, I_{s,2}, R_1, R_2) \in R_+^{12} : \tag{6}
$$

$$
0 \leqslant \sum_i S_i + \sum_i E_i + \sum_i V_i + \sum_i I_{a,i} + \sum_i I_{s,i} + \sum_i R_i \leqslant 1, i = \overline{1,2} \Big\}.
$$

Theorem 1. Consider system (3) with initial conditions (4).

The set Ω is an attracting and positively invariant with respect to model (3), with $S_i, V_i, R_i \; (i = \overline{1,2})$; remaining positive. The total population in each patch is assumed to be constant, and all their pathological states are also bounded.

Proof. Under initial conditions (4):

- In the event that E_1 becomes zero at t_1 before E_2 becomes zero, then at t_1, we have

$$
\frac{dE_1}{dt} = c_1 (I_{a,1} + I_{s,1}) S_1 + \varphi_{21}^E E_2 \geqslant 0.
$$

  This demonstrates that E_1 is a nondecreasing function of t at t_1. Hence, E_1 stays nonnegative. Analogously, the same holds for E_2.

- In the event that $I_{a,1}$ becomes zero at some time t_2 before $I_{a,2}$ becomes zero, then at t_2, we have

$$
\frac{dI_{a,1}}{dt} = \beta_1 E_1 + \varphi_{21}^{I_a} I_{a,2} \geqslant 0.
$$

  This demonstrates that $I_{a,1}$ is a nondecreasing function of t at t_2. Hence, $I_{a,1}$ stays nonnegative. Analogously, the same holds for $I_{a,2}$.

- In the event that $I_{s,1}$ becomes zero at some time t_3 before $I_{s,2}$ becomes zero, then at t_3, we have

$$\frac{dI_{s,1}}{dt} = \beta_2 E_1 \geqslant 0.$$

This demonstrates that $I_{s,1}$ is a nondecreasing function of t at t_3. Hence, $I_{s,1}$ stays nonnegative. Analogously, the same holds for $I_{s,2}$.

- Suppose now that at some time t_4, $S_1(t_4) = 0$ before S_2 goes to zero. Then at $t = t_4$, from system (3), we have

$$\frac{dS_1}{dt} = \mu \frac{N_1}{N} + \varphi_{21}^S S_2 + \lambda_2 V_1 + \gamma R_1 > 0,$$

which implies that $\dfrac{dS_1}{dt} > 0$ when $\dfrac{N_1}{N}$ is strictly positive.

Thus, there is no time t_4 such that $S_1(t_4) = 0$. Therefore, S_1 stays positive for $t > 0$ when the initial condition $S_1(0) > 0$. Using comparable reasoning, we deduce the positivity of S_2.

- Likewise at some time t_5, $V_1(t_5) = 0$ before V_2 goes to zero. Then at $t = t_5$, from system (3), we have

$$\frac{dV_1}{dt} = \lambda_1 S_1 + \lambda_3 E_1 + \lambda_4 I_{a,1} + \varphi_{21}^V V_2 > 0,$$

which implies that $\dfrac{dV_1}{dt} > 0$ because $S_1(t) > 0$ for $t > 0$.

Thus, there is no time t_5 such that $V_1(t_5) = 0$. Therefore, V_1 stays positive. Using comparable reasoning, we deduce the positivity of V_2.

- Likewise at some time t_6; $R_1(t_6)$ before R_2 goes to zero. Then at $t = t_6$, from system (3), we have

$$\frac{dR_1}{dt} = \gamma_1 I_{a,1} + \gamma_2 I_{s,1} + \lambda_5 V_1 + \varphi_{21}^R R_2 > 0,$$

which implies that $\dfrac{dR_1}{dt} > 0$ because $V_1(t) > 0$ for $t > 0$.

Thus, there is no time t_6 such that $R_1(t_6) = 0$. Therefore, R_1 stays positive. Using comparable reasoning, we deduce the positivity of R_2.

Since the positive set Ω is invariant under system (3) and the total population in each patch $(N_i)_{i=1,2}$ is assumed to be constant, and all their pathological states are also bounded. $\qquad\square$

4.2 Disease-Free Equilibrium

The DFE (disease-free equilibrium) of system (3) is expressed as

$$\mathcal{E}_0^* = \left(S_1^* \ S_2^* \ 0 \ 0 \ V_1^* \ V_2^* \ 0 \ 0 \ 0 \ 0 \ R_1^* \ R_2^* \right)^T, \tag{7}$$

where

$$
\begin{cases}
S_1^* = \dfrac{\mu k_2 k_3 \left(n_1 \left(d_1 + d_3\right) + d_1 n_2\right)}{d_3 \left(d_3 + d_1 + d_2\right)}, \\[2mm]
S_2^* = \dfrac{\mu k_2 k_3 \left(d_2 n_1 + \left(d_2 + d_3\right) n_2\right)}{d_3 \left(d_3 + d_1 + d_2\right)}, \\[2mm]
V_1^* = \dfrac{\lambda_1 \left(\varphi_{21}^V + c_4\right) \mu k_2 k_3 \left(n_1 \left(d_1 + d_3\right) + d_1 n_2\right)}{k_2 d_3 \left(d_3 + d_1 + d_2\right)} \\[2mm]
\quad\quad + \dfrac{\lambda_1 \varphi_{21 k_2}^V \mu k_2 k_3 \left(d_2 n_1 + \left(d_2 + d_3\right) n_2\right)}{d_3 \left(d_3 + d_1 + d_2\right)}, \\[2mm]
V_2^* = \dfrac{\lambda_1 \varphi_{12}^V \mu k_2 k_3 \left(n_1 \left(d_1 + d_3\right) + d_1 n_2\right)}{k_2 d_3 \left(d_3 + d_1 + d_2\right)} \\[2mm]
\quad\quad + \dfrac{\lambda_1 \left(\varphi_{12}^V + c_4\right) \mu k_2 k_3 \left(d_2 n_1 + \left(d_2 + d_3\right) n_2\right)}{k_2 d_3 \left(d_3 + d_1 + d_2\right)}, \\[2mm]
R_1^* = \dfrac{\lambda_5 \lambda_1 k_4 \mu k_2 k_3 \left(n_1 \left(d_1 + d_3\right) + d_1 n_2\right)}{k_2 k_3 d_3 \left(d_3 + d_1 + d_2\right)} \\[2mm]
\quad\quad + \dfrac{\mu k_2 k_3 \lambda_5 \lambda_1 \left(\varphi_{21}^V k_3 + \varphi_{21}^R k_5\right) \left(d_2 n_1 + \left(d_2 + d_3\right) n_2\right)}{k_2 k_3 d_3 \left(\varphi_{12}^R + c_7\right) \left(d_3 + d_1 + d_2\right)}, \\[2mm]
R_2^* = \dfrac{\mu k_2 k_3 \lambda_1 \lambda_5 \left(\varphi_{12}^V k_3 + \varphi_{12}^R k_4\right) \left(n_1 \left(d_1 + d_3\right) + d_1 n_2\right)}{k_2 k_3 d_3 \left(\varphi_{21}^R + c_7\right) \left(d_3 + d_1 + d_2\right)} \\[2mm]
\quad\quad + \dfrac{\lambda_5 \lambda_1 k_5 \mu k_2 k_3 \left(d_2 n_1 + \left(d_2 + d_3\right) n_2\right)}{k_2 k_3 d_3 \left(d_3 + d_1 + d_2\right)},
\end{cases}
$$

and

$$
\begin{cases}
d_1 = \gamma \lambda_1 \lambda_5 k_6 + \lambda_1 \lambda_2 k_3 \varphi_{21}^V + k_3 k_2 \varphi_{21}^S, \\[1mm]
d_2 = \gamma \lambda_1 \lambda_5 k_7 + \lambda_1 \lambda_2 k_3 \varphi_{12}^V + k_2 k_3 \varphi_{12}^S, \\[1mm]
d_3 = k_3 k_2 \mu + \lambda_1 \mu \left(\lambda_5 + c_7\right) \left(k_6 + k_7 + c_4 c_7\right),
\end{cases}
\tag{8}
$$

and

$$
\begin{cases}
k_2 = c_4^2 + \varphi_{12}^V c_4 + \varphi_{21}^V c_4, \\
k_3 = c_7^2 + \varphi_{12}^R c_7 + \varphi_{21}^R c_7, \\
k_4 = \left(\varphi_{21}^V + c_4\right)\left(\varphi_{21}^R + c_7\right) + \varphi_{12}^V \varphi_{21}^R, \\
k_5 = \left(\varphi_{12}^V + c_4\right)\left(\varphi_{12}^R + c_7\right) + \varphi_{12}^R \varphi_{21}^V, \\
k_6 = \varphi_{21}^V \left(\varphi_{21}^R + c_7\right) + \varphi_{21}^R \left(\varphi_{12}^V + c_4\right), \\
k_7 = \varphi_{12}^V \left(\varphi_{12}^R + c_7\right) + \varphi_{12}^R \left(\varphi_{21}^V + c_4\right).
\end{cases}
\tag{9}
$$

The existence of the DFE $\mathcal{E}_0^*$ remains unaffected by any prerequisites regarding positive operational data.

4.3 Vaccination reproduction number R_v of two-patch metapopulation

In this subsection, we present the method used for our SEIR-V model to estimate the vaccination reproduction number R_v. This method is proposed by Diekmann, Heesterbeek, and Metz [26] and elaborated by Van Den Driessche and Watmough [27, 25], which gives a way of determining R_v for an ordinary differential equation compartmental model by using the next-generation matrix.

Let $X = (E_1, E_2, I_{a,1}, I_{a,2}, I_{s,1}, I_{s,2})^T$. Then the system can be written as

$$
\frac{dX}{dt} = \mathcal{F}(X) - \mathcal{V}(X),
$$

where

$$
\mathcal{F}(X) = \begin{pmatrix}
c_1 \left(I_{a,1} + I_{s,1}\right) S_1 \\
c_2 \left(I_{a,2} + I_{s,2}\right) S_2 \\
0 \\
0 \\
0 \\
0
\end{pmatrix},
$$

and

$$\mathcal{V}(X) = \begin{pmatrix} -\varphi_{21}^E E_2 + \left(\varphi_{12}^E + c_3\right) E_1 \\ -\varphi_{12}^E E_1 + \left(\varphi_{21}^E + c_3\right) E_2 \\ -\beta_1 E_1 - \varphi_{21}^{I_a} I_{a,2} + \left(\varphi_{12}^{I_a} + c_5\right) I_{a,1} \\ -\beta_1 E_2 - \varphi_{12}^{I_a} I_{a,1} + \left(\varphi_{21}^{I_a} + c_5\right) I_{a,2} \\ -\beta_2 E_1 + c_6 I_{s,1} \\ -\beta_2 E_2 + c_6 I_{s,2} \end{pmatrix}.$$

The basic reproduction number, R_v, is calculated by next generation technique. The F and V matrices at the DFE $\mathcal{E}_0^*$ is given as follows:

$$F = \left.\frac{\partial \mathcal{F}(X)}{\partial X}\right|_{\mathcal{E}_0^*} = \begin{pmatrix} 0 & 0 & c_1 S_1^* & 0 & c_1 S_1^* & 0 \\ 0 & 0 & 0 & c_2 S_2^* & 0 & c_2 S_2^* \\ 0 & 0 & 0 & 0 & 0 & 0 \\ 0 & 0 & 0 & 0 & 0 & 0 \\ 0 & 0 & 0 & 0 & 0 & 0 \\ 0 & 0 & 0 & 0 & 0 & 0 \end{pmatrix},$$

and

$$V = \left.\frac{\partial \mathcal{V}(X)}{\partial X}\right|_{\mathcal{E}_0^*} = \begin{pmatrix} \varphi_{12}^E + c_3 & -\varphi_{21}^E & 0 & 0 & 0 & 0 \\ -\varphi_{12}^E & \varphi_{21}^E + c_3 & 0 & 0 & 0 & 0 \\ -\beta_1 & 0 & \varphi_{12}^{I_a} + c_5 & -\varphi_{21}^{I_a} & 0 & 0 \\ 0 & -\beta_1 & -\varphi_{12}^{I_a} & \varphi_{21}^{I_a} + c_5 & 0 & 0 \\ -\beta_2 & 0 & 0 & 0 & c_6 & 0 \\ 0 & -\beta_2 & 0 & 0 & 0 & c_6 \end{pmatrix}.$$

Therefore, the next generation matrix is

$$FV^{-1} = \begin{pmatrix} m_1 S_1^* & m_3 S_1^* & \frac{c_1\left(c_5 + \varphi_{21}^{I_a}\right)}{k_1} S_1^* & \frac{c_1 \varphi_{21}^{I_a}}{k_1} S_1^* & \frac{c_1}{c_6} S_1^* & 0 \\ m_2 S_2^* & m_4 S_2^* & \frac{c_2 \varphi_{12}^{I_a}}{k_1} S_2^* & \frac{c_2\left(c_5 + \varphi_{12}^{I_a}\right)}{k_1} S_2^* & 0 & \frac{c_2}{c_6} S_2^* \\ 0 & 0 & 0 & 0 & 0 & 0 \\ 0 & 0 & 0 & 0 & 0 & 0 \\ 0 & 0 & 0 & 0 & 0 & 0 \\ 0 & 0 & 0 & 0 & 0 & 0 \end{pmatrix},$$

where

$$m_1 = c_1 \left(\frac{\left(c_3 + \varphi_{21}^E\right)}{k_0} \left(\frac{\beta_2}{c_6} + \frac{c_5 \beta_1}{k_1} \right) + \frac{\beta_1 \varphi_{21}^{I_a}}{c_3 k_1} \right),$$

$$m_2 = c_2 \left(\frac{\varphi_{12}^E}{k_0} \left(\frac{\beta_2}{c_6} + \frac{c_5 \beta_1}{k_1} \right) + \frac{\beta_1 \varphi_{12}^{I_a}}{c_3 k_1} \right),$$

$$m_3 = c_1 \left(\frac{\varphi_{21}^E}{k_0} \left(\frac{\beta_2}{c_6} + \frac{c_5 \beta_1}{k_1} \right) + \frac{\beta_1 \varphi_{21}^{I_a}}{c_3 k_1} \right),$$

$$m_4 = c_2 \left(\frac{\left(c_3 + \varphi_{12}^E\right)}{k_0} \left(\frac{\beta_2}{c_6} + \frac{c_5 \beta_1}{k_1} \right) + \frac{\beta_1 \varphi_{12}^{I_a}}{c_3 k_1} \right),$$

and

$$k_0 = c_3 \varphi_{12}^E + c_3 \varphi_{21}^E + c_3^2,$$
$$k_1 = c_5 \varphi_{12}^{I_a} + c_5 \varphi_{21}^{I_a} + c_5^2.$$

The reproduction number, R_v, is the spectral radius of the next generation matrix, which is given by

$$R_v = \frac{1}{2} \frac{\mu k_2 k_3}{d_3 \left(d_3 + d_1 + d_2\right)} \left(\left(d_1 + n_1 d_3\right) m_1 + \left(d_2 + n_2 d_3\right) m_4 \right.$$
$$\left. + \sqrt{\left(\left(d_1 + n_1 d_3\right) m_1 - \left(d_2 + n_2 d_3\right) m_4\right)^2 + 4 m_2 m_3 \left(d_1 + n_1 d_3\right) \left(d_2 + n_2 d_3\right)} \right),$$

where (c_i) and (d_i) are defined in (5) and (8), respectively.

4.4 Model analysis

Theorem 2. If $R_v < 1$, then the DFE $\mathcal{E}_0^*$ is locally asymptotically stable and unstable otherwise.

Proof. System (3) has a unique DFE point $\mathcal{E}_0^*$ in the set Ω, given in (7).

The eigenvalues of the Jacobian matrix at the DFE point $\mathcal{E}_0^*$ are given by

$$\begin{cases} \rho_1 = \rho_2 = -c_6, \\ \rho_3 = -\left(\varphi_{12}^E + \varphi_{21}^E + c_3\right), \\ \rho_4 = -c_3, \\ \rho_5 = -\left(c_5 + \varphi_{12}^{I_a} + \varphi_{21}^{I_a}\right), \\ \rho_6 = -c_5, \end{cases}$$

where $(\rho_i)_{i=7,12}$ are roots of

$$P\left(Z\right) = Z^6 + C_5 Z^5 + C_4 Z^4 + C_3 Z^3 + C_2 Z^2 + C_1 Z + C_0.$$

By using Lienard–Chipart criteria, the DFE point $\mathcal{E}_0^*$ is locally asymptotically stable if the coefficients C_5, C_4, C_3, C_2, C_1, and C_0 are positive and their Hurwitz's determinants are positive. It shows that the positivity of Hurwitz determinants is very complicated to achieve. However, the computational cost can be reduced by using the simplified version mentioned in [5, 17]. That is, the coefficients that must be computed are C_5, C_4, C_3, C_2, C_1, and C_0 only. Note that C_5, C_4, and C_3 are needed because the simplified version of Lienard–Chipart criteria still require $|H_2| = C_5 C_4 - C_3 > 0$ [11].

Indeed, we employed formal calculation software (Maxima Version 5.42.1) to establish that if $R_v < 1$, then all $(C_i)_{i=\overline{0,5}}$ and $|H_2|$ are positive. $\qquad\square$

Theorem 3. If $R_v < 1$, then the the DFE $\mathcal{E}_0^*$ is globally asymptotically stable in Ω.

Proof. Since for $i = 1,2$, we have

$$S_1 \leqslant S_1^*, S_2 \leqslant S_2^*,$$

$$\begin{cases}
\dfrac{dE_1}{dt} \leqslant -\left(\varphi_{12}^E + c_3\right) E_1 + \varphi_{21}^E E_2 + c_1 S_1^* I_{a,1} + c_1 S_1^* I_{s,1}, \\[2mm]
\dfrac{dE_2}{dt} \leqslant \varphi_{12}^E E_1 - \left(\varphi_{21}^E + c_3\right) E_2 + c_2 S_2^* I_{a,2} + c_2 S_2^* I_{s,2}, \\[2mm]
\dfrac{dI_{a,1}}{dt} \leqslant \beta_1 E_1 - \left(\varphi_{12}^{I_a} + c_5\right) I_{a,1} + \varphi_{21}^{I_a} I_{a,2}, \\[2mm]
\dfrac{dI_{a,2}}{dt} \leqslant \beta_1 E_2 + \varphi_{12}^{I_a} I_{a,1} - \left(\varphi_{21}^{I_a} + c_5\right) I_{a,2}, \\[2mm]
\dfrac{dI_{s,1}}{dt} \leqslant \beta_2 E_1 - c_6 I_{s,1}, \\[2mm]
\dfrac{dI_{s,2}}{dt} \leqslant \beta_2 E_2 - c_6 I_{s,2}.
\end{cases} \qquad (10)$$

Defining an auxiliary linear system using the right-hand side of system (10), we have

$$
\begin{cases}
\dfrac{d\widetilde{E}_1}{dt} = -\left(\varphi_{12}^E + c_3\right)\widetilde{E}_1 + \varphi_{21}^E \widetilde{E}_2 + c_1 S_1^* \widetilde{I}_{a,1} + c_1 S_1^* \widetilde{I}_{s,1}, \\[2mm]
\dfrac{d\widetilde{E}_2}{dt} = \varphi_{12}^E \widetilde{E}_1 - \left(\varphi_{21}^E + c_3\right)\widetilde{E}_2 + c_2 S_2^* \widetilde{I}_{a,2} + c_2 S_2^* \widetilde{I}_{s,2}, \\[2mm]
\dfrac{d\widetilde{I}_{a,1}}{dt} = \beta_1 \widetilde{E}_1 - \left(\varphi_{12}^{I_a} + c_5\right)\widetilde{I}_{a,1} + \varphi_{21}^{I_a} \widetilde{I}_{a,2}, \\[2mm]
\dfrac{d\widetilde{I}_{a,2}}{dt} = \beta_1 \widetilde{E}_2 + \varphi_{12}^{I_a} I_{a,1} - \left(\varphi_{21}^{I_a} + c_5\right)\widetilde{I}_{a,2}, \\[2mm]
\dfrac{d\widetilde{I}_{s,1}}{dt} = \beta_2 \widetilde{E}_1 - c_6 \widetilde{I}_{s,1}, \\[2mm]
\dfrac{d\widetilde{I}_{s,2}}{dt} = \beta_2 \widetilde{E}_2 - c_6 \widetilde{I}_{s,2},
\end{cases}
$$

or, in other words,

$$
\frac{d}{dt}\left(\widetilde{E}_1 \ \widetilde{E}_2 \ \widetilde{I}_{a,1} \ \widetilde{I}_{a,2} \ \widetilde{I}_{s,1} \ \widetilde{I}_{s,2}\right)^T
$$

$$
= \begin{pmatrix}
-\left(\varphi_{12}^E + c_3\right) & \varphi_{21}^E & c_1 S_1^* & 0 & c_1 S_1^* & 0 \\
\varphi_{12}^E & -\left(\varphi_{21}^E + c_3\right) & 0 & c_2 S_2^* & 0 & c_2 S_2^* \\
\beta_1 & 0 & -\left(\varphi_{12}^{I_a} + c_5\right) & 0\varphi_{21}^{I_a} & 0 & 0 \\
0 & \beta_1 & \varphi_{12}^{I_a} & -\left(\varphi_{21}^{I_a} + c_5\right) & 0 & 0 \\
\beta_2 & 0 & 0 & 0 & -c_6 & 0 \\
0 & \beta_2 & 0 & 0 & 0 & -c_6
\end{pmatrix}
\begin{pmatrix}
\widetilde{E}_1 \\
\widetilde{E}_2 \\
\widetilde{I}_{a,1} \\
\widetilde{I}_{a,2} \\
\widetilde{I}_{s,1} \\
\widetilde{I}_{s,2}
\end{pmatrix}.
$$

So,

$$
\frac{d}{dt}\begin{pmatrix}
d\widetilde{E}_1 \\
d\widetilde{E}_2 \\
d\widetilde{I}_{a,1} \\
d\widetilde{I}_{a,2} \\
d\widetilde{I}_{s,1} \\
d\widetilde{I}_{s,2}
\end{pmatrix} = (F - V)\begin{pmatrix}
d\widetilde{E}_1 \\
d\widetilde{E}_2 \\
d\widetilde{I}_{a,1} \\
d\widetilde{I}_{a,2} \\
d\widetilde{I}_{s,1} \\
d\widetilde{I}_{s,2}.
\end{pmatrix}. \tag{11}
$$

We have $R_v < 1 \iff \sigma(F - V) < 0$, where $\sigma(F - V)$ is the spectral abscissa of the matrix $F - V$ (see the proof of Theorem 2 [26]). So, when $R_v < 1$, the eigenvalues of $(F - V)$ are with negative real parts. Thus all nonnegative solutions of (11) are such that

$$
\lim_{t \longrightarrow +\infty}\left(\widetilde{E}_1, \widetilde{E}_2, \widetilde{I}_{a,1}, \widetilde{I}_{a,2}, \widetilde{I}_{s,1}, \widetilde{I}_{s,2}\right) = (0, 0, 0, 0, 0, 0).
$$

By a standard comparison principle (see [24, Theorem B.1]) and the non-negativity of $(E_1, E_2, I_{a,1}, I_{a,2}, I_{s,1}, I_{s,2})$, we conclude that when $R_v < 1$, all nonnegative solutions of (3) satisfy

$$\lim_{t \longrightarrow +\infty} (E_1, E_2, I_{a,1}, I_{a,2}, I_{s,1}, I_{s,2}) = (0, 0, 0, 0, 0, 0). \tag{12}$$

Since (12) is satisfied, (3) is an asymptotically autonomous system [see [8, Theorem 2.5]] with limit affine system

$$\begin{cases} \dfrac{dS_1}{dt} = \mu + \varphi_{21}^S S_2 - \left(\varphi_{12}^S + c_0\right) S_1 + \lambda_2 V_1 + \gamma R_1, \\[2mm] \dfrac{dS_2}{dt} = \mu + \varphi_{12}^S S_1 - \left(\varphi_{21}^S + c_0\right) S_2 + \lambda_2 V_2 + \gamma R_2, \\[2mm] \dfrac{dV_1}{dt} = \lambda_1 S_1 + \varphi_{21}^V V_2 - \left(\varphi_{12}^V + c_4\right) V_1, \\[2mm] \dfrac{dV_2}{dt} = \lambda_1 S_2 + \varphi_{12}^V V_1 - \left(\varphi_{21}^V + c_4\right) V_2, \\[2mm] \dfrac{dR_1}{dt} = \lambda_5 V_1 + \varphi_{21}^R R_2 - \left(\varphi_{12}^R + c_7\right) R_1, \\[2mm] \dfrac{dR_2}{dt} = \lambda_5 V_2 + \varphi_{12}^R R_1 - \left(\varphi_{21}^R + c_7\right) R_2. \end{cases} \tag{13}$$

It is easy to verify from (13) that

$$\lim_{t \longrightarrow +\infty} (S_1, S_2, V_1, V_2, R_1, R_2) = (S_1^*, S_2^*, V_1^*, V_2^*, R_1^*, R_2^*).$$

The globally asymptotic stability of the DFE $\mathcal{E}_0^*$ is then proved if $R_v < 1$. $\square$

The presence of endemic equilibrium, characterized by positive infective numbers, has barely been discussed here. Although their existence has not been formally proven, numerical simulations suggest a globally asymptotically stable equilibrium when $R_v > 1$. Investigating the system's persistence properties under the condition $R_v > 1$ would be a valuable avenue for further exploration.

Lemma 1. [30] Let $\phi_t : X \to X$ be a semiflow and let $X_0 \subset X$ be an open set. Define $\partial X_0 = X \smallsetminus X_0$ and $M_\partial = \{x \in \partial X_0 : \phi_t x \in \partial X_0, t \geqslant 0\}$. Assume the following conditions:

1. $\phi_t X_0 \subset X_0$ and ϕ_t has a global attractor A.

2. There exists a finite sequence $\mathcal{M} = \{M_1, \ldots, M_k\}$ of disjoint, compact, and isolated invariant sets in ∂X_0 such that

   (a) $\Omega\left(M_\partial\right) := \cup_{x \in M_\partial} w\left(x\right) \subset \cup_{i=1}^k M_i$.

   (b) No subset of $\mathcal{M}$ forms a cycle in ∂X_0.

   (c) M_i is isolated in X.

   (d) $W^s\left(M_i\right) \cap X_0 = \emptyset$, where $W^s\left(M_i\right) = \{x \in X_0 : w\left(x\right) \subset M_i\}$ for each $1 \leqslant i \leqslant k$.

Then ϕ_t is uniformly persistent with respect to $(X_0, \partial X_0)$, that is, there exists $\theta > 0$ such that

$$\lim_{t \longrightarrow +\infty} \inf d\left(\phi_t x, \partial X_0\right) \geqslant \theta \ \ \text{for} \ \ x \in X_0.$$

Therefore, we have the following result.

Theorem 4. If $R_v > 1$, then system (3) is uniformly persistent, namely, there exists a constant $\theta > 0$ such that

$$\lim_{t \longrightarrow +\infty} \inf S_i\left(t\right) > \theta, \ \lim_{t \longrightarrow +\infty} \inf E_i\left(t\right) > \theta, \ \lim_{t \longrightarrow +\infty} \inf V_i\left(t\right) > \theta,$$
$$\lim_{t \longrightarrow +\infty} \inf I_{a,i}\left(t\right) > \theta, \ \lim_{t \longrightarrow +\infty} \inf I_{s,i}\left(t\right) > \theta, \ \lim_{t \longrightarrow +\infty} \inf R_i\left(t\right) > \theta,$$

for any initial conditions satisfying (4).

Proof. Choose

$$\begin{cases} X = \Omega \\ X_0 = \big\{(S_1, S_2, E_1, E_2, V_1, V_2, I_{a,1}, I_{a,2}, I_{s,1}, I_{s,2}, R_1, R_2) \in X : \\ E_1 + E_2 > 0, I_{a,1} + I_{a,2} > 0, I_{s,1} + I_{s,2} > 0 \big\}, \end{cases}$$

and

$$\begin{aligned} \partial X_0 &= X \setminus X_0 \\ &= \Big\{(S_1, S_2, E_1, E_2, V_1, V_2, I_{a,1}, I_{a,2}, I_{s,1}, I_{s,2}, R_1, R_2) \in X : \\ &\qquad E_1 = E_2 = I_{a,1} = I_{a,2} = I_{s,1} = I_{s,2} = 0 \Big\}. \end{aligned}$$

Let ϕ_t be the semi flow induced by the solutions of system (3).

We have proved in Theorem 1 that $\phi_t X_0 \subset X_0$ and ϕ_t is ultimately bounded in X_0; so there always exists a global attractor for ϕ_t. It is obvious

that $\mathcal{E}_0^*$ is the unique boundary equilibrium on ∂X_0, which implies that $\mathcal{E}_0^*$ is globally stable on ∂X_0. Moreover, $(S_1, S_2, , V_1, V_2, R_1, R_2)$ converges to $(S_1^*, S_2^*, , V_1^*, V_2^*, R_1^*, R_2^*)$ on ∂X_0.

Let $M_1 = \{\mathcal{E}_0^*\}$ and $\mathcal{M} = \{M_1\}$, then $\cup_{x \in M_\partial} w(x) = M_1$ and no subset of $\mathcal{M}$ forms a cycle in ∂X_0.

If $R_v > 1$, then $\mathcal{E}_0^*$ is unstable in X_0. Therefore, conditions $(2 - c)$ and $(2 - d)$ of Lemma 1 are satisfied. Then ϕ_t is uniformly persistent with respect to $(X_0, \partial X_0)$, that is, there exists $\theta > 0$ such that

$$\lim_{t \longrightarrow +\infty} \inf d(\phi_t x, \partial X_0) \geqslant \theta \ \text{ for } \ x \in X_0.$$

We have thus shown that if $R_v > 1$, then the disease is endemic. $\square$

5 Numerical simulation

In this section, we extend our exploration into the numerical simulation of COVID-19 transmission within a two-patch framework, leveraging well-established methodologies commonly employed in epidemiological studies. Building upon the model detailed and examined in Section 4, our objective is to unravel the intricate dynamics of COVID-19 transmission influenced by migration, vaccination, and medical unavailability.

In a prior study [7], we investigated disease transmission dynamics in the absence of migration in a single patch. In the current work, which builds upon our earlier research, we now consider the pivotal role of migration—representing the movement of individuals between patches. Migration rates, denoted by φ_{12} and φ_{21}, exert a substantial influence on the overall transmission dynamics.

To ground our simulations in real-world scenarios, we integrate data from Table 1 into our analysis. Additionally, we set migration rates from the patch 1 to the patch 2 ($\varphi_{12}^S, \ \varphi_{12}^E, \ \varphi_{12}^V, \ \varphi_{12}^{I_a}, \ \varphi_{12}^R$) at 0.001 and migration rates from the patch 2 to the patch 1 ($\varphi_{21}^S, \ \varphi_{21}^E, \ \varphi_{21}^V, \ \varphi_{21}^{I_a}, \ \varphi_{21}^R$) at 0.005. These rates underscore the interconnectedness of patches and contribute to the comprehensive understanding of disease spread across different regions.

Table 1: The operational parameters of the simulation consist of two categories: those characterizing the population and the disease remain the same across all patches, whereas parameters reflecting the behavior of individuals vary from one patch to another

Parameters	Description	Values (per day)
N	Population size	100000
N_1	Population size in patch 1 (Most populated patch).	75000
N_2	Population size in patch 2 (Least populated patch).	25000
μ	Recruitment rate.	3.38e-05
α_1	Infection rate for unconfined persons.	0.01-0.3
α_2	Infection rate for confined persons.	0.01-0.3
η_1	The confinement rate in patch 1.	0.2-0.5
η_2	The confinement rate in patch 2.	0.2-0.5
β_1	Rate of an exposed becoming asymptomatic infected.	0.092
β_2	Rate of an exposed becoming symptomatic infected.	0.05
λ_1	Vaccination rate of susceptible.	0.01-0.03
λ_2	The ineffectiveness rate of the vaccine	0.001765
λ_3	Vaccination rate of exposed persons.	0.00167
λ_4	Vaccination rate of asymptomatic infected.	0.0167
λ_5	The effectiveness rate of the vaccine.	0.008
γ	Rate of a recovered becoming susceptible.	0.0099
γ_1	The recovery rate of asymptomatic people	0.01
γ_2	the recovery rate of symptomatic people	0.0005
δ	COVID-19 death rate.	0.0055

Our simulation parameters encompass scenarios without migration restrictions, incorporating measures such as containment and vaccination strategies. The outcomes of these simulations gauged through R_v and other pertinent metrics, offer valuable insights into the potential efficacy of interventions aimed at curtailing the virus's propagation.

Subsequently, we delve into an analysis of the sensitivity of key parameters to the vaccine reproduction number R_v. Following this, we meticulously scrutinize the theoretical results previously obtained, aiming to provide empirical substantiation and validate the accuracy of our theoretical framework.

This multifaceted approach enhances our understanding of the practical implications of proposed interventions and reinforces the robustness of our theoretical foundation.

5.1 Sensitivity analysis of the main parameters on R_v

To effectively mitigate the impact of COVID-19 and reduce associated fatalities, understanding the relative importance of various parameters influencing its progression is crucial. The vaccination reproduction number, R_v [10], stands out as a key determinant in the transmission dynamics of COVID-19.

Our investigation employs sensitivity analysis on R_v within the framework of our model (3). This analysis aims to discern the individual importance of each parameter, shedding light on influential factors in disease transmission. The derived sensitivity indices offer insights into how a state variable changes relative to variations in specific parameters.

Sensitivity analysis, a widely used technique, involves computing the first-order partial derivatives of model output concerning input parameters. This process can be conceptualized as calculating gradients in a multidimensional reference parameter space [23], providing valuable information on the model's responsiveness to slight changes in input parameters.

The normalized forward sensitivity index of R_v, denoted as $\mathcal{I}_p^{R_v}$, quantifies the sensitivity with respect to a given parameter p and is defined by the expression:

$$\mathcal{I}_p^{R_v} = \frac{\partial R_v}{\partial p} \frac{p}{R_v}.$$

This index facilitates a quantitative assessment of how alterations in individual parameters influence the value of R_v, a pivotal metric for understanding disease transmission. By leveraging explicit formulas for each parameter affecting R_v, as detailed in reference [31], we gain precise insights into the impact of specific parameters on R_v. Such sensitivity analysis proves invaluable in prioritizing interventions and control measures to effectively curtail the spread of the disease, enabling a more targeted and comprehensive approach to managing COVID-19.

Table 2: Local sensitivity indices for R_v concerning parameters in the proposed model are computed at the baseline parameter values provided in Table 1. Parameters exhibiting the highest sensitivity are highlighted in bold

Parameters	α_1	$\boldsymbol{\alpha_2}$	η_1	η_2	$\boldsymbol{\beta_1}$	$\boldsymbol{\beta_2}$	$\boldsymbol{\lambda_1}$
Sensitivity Index	0.11	**0.89**	-0.11	-0.00006	**-0.34**	**0.37**	**-0.18**

Parameters	λ_2	λ_3	λ_4	λ_5	γ	γ_1	γ_2
Sensitivity Index	0.032	-0.016	-0.018	0.066	0.079	-0.11	-0.059

Parameters	φ_{21}^S	φ_{21}^E	φ_{21}^V	$\varphi_{21}^{I_a}$	φ_{21}^R
Sensitivity Index	0.15	0.0003	0.008	0.002	0.009

Parameters	φ_{12}^S	φ_{12}^E	φ_{12}^V	$\varphi_{12}^{I_a}$	φ_{12}^R
Sensitivity Index	-0.15	-0.006	-0.008	-0.009	-0.009

Table 2 highlights the parameters most responsive to changes in the vaccination reproduction number (R_v), with the transmission probability of unconfined individuals (α_2) and the transition rate from exposed to symptomatic infected (β_2) exhibiting the highest sensitivity. The vaccination rate (λ_1) and the transition rate from exposed to asymptomatic infected (β_1) closely follow in significance. A 10% increase (or decrease) in α_2 or β_2 leads to corresponding 8.9% and 3.7% changes in R_v, respectively, as denoted by $\mathcal{I}_{\alpha_1}^{R_v} = +0.89$ and $\mathcal{I}_{\eta_1}^{R_v} = +0.37$. Conversely, a 10% increase in λ_1 or β_1 corresponds to a 1.8% and 3.4% decrease in R_v, respectively, indicated by $\mathcal{I}_{\lambda_1}^{R_v} = -0.18$ and $\mathcal{I}_{\beta_1}^{R_v} = -0.34$.

The local analysis emphasizes the importance of implementing effective containment measures for managing the transmission probability (α_2) and the transition rate from exposed to symptomatic infected. This involves stringent containment measures, the use of physical barriers, and adherence to social distancing guidelines. Additionally, vaccination efforts, represented by the rate (λ_1), play a crucial role in reducing the spread of the disease. By strategically controlling these parameters, a significant reduction in COVID-19-related deaths can be achieved.

5.2 The stability of the DFE

In this subsection, we will confirm the theoretical results obtained earlier through numerical simulations for the following parameter values (per day):

$$\alpha_1 = 0.010 \; ; \; \alpha_2 = 0.0655 \; ; \; \eta_1 = 0.20 \; ; \; \eta_2 = 0.25 \; ; \; \lambda_1 = 0.01817.$$

The existence and stability conditions in Theorem 2 are satisfied

$$R_v = 0.8375 < 1.$$

Hence, system (3) has a DFE,

$$\begin{aligned}
\mathcal{E}_0^* &= \begin{bmatrix} S_1^*, \; S_2^*, \; E_1^*, \; E_2^*, \; V_1^*, \; V_2^*, \; I_{a,1}^*, \; I_{a,2}^*, \; I_{s,1}^*, \; I_{s,2}^* \; , \; R_1^*, \; R_2^* \end{bmatrix}^T \\
&= \begin{bmatrix} 0.1915, \; 0.0385, \; 0, \; 0, \; 0.3326, \; 0.0713, \; 0, \; 0, \; 0, \; 0, \; 0.2861, \; 0.0573 \end{bmatrix}^T .
\end{aligned}$$

Therefore, the DFE $\mathcal{E}_0^*$ is stable. This also implies that the disease is eradicated, as depicted in Figures 2 and 3.

Furthermore, if we increase the values of the most sensitive parameters such as $\alpha_1 = 0.0653$, $\alpha_2 = 0.1295$, $\eta_1 = 0.20$, $\eta_2 = 0.30$ and $\lambda_1 = 0.00117$, through direct calculation, the vaccination reproduction number $R_v = 6.4251 > 1$. Consequently, according to Theorem 2, the DFE is unstable, and the model (3) has an endemic equilibrium.
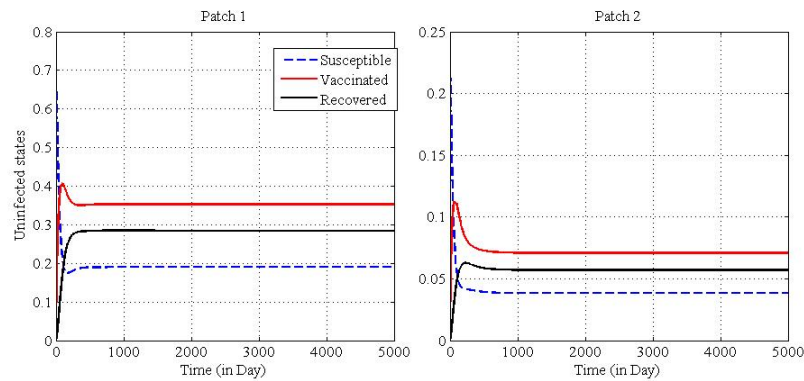

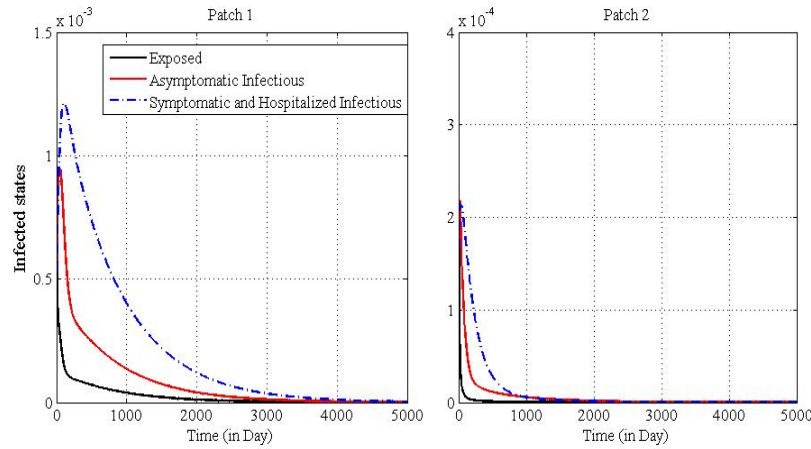Figure 2: The proposed model has only one DFE $\mathcal{E}_0^*$, which is asymptotically stable when $R_v < 1$.

Figure 3: The proposed model has only one DFE $\mathcal{E}_0^*$, which is asymptotically stable when $R_v < 1$.

5.3 The existence and stability of the endemic equilibrium of the model

Now, we deal with the existence of endemic equilibrium of model (3). Consider the following parameter values (per day):

$$\alpha_1 = 0.0653, \ \alpha_2 = 0.1295, \ \eta_1 = 0.20, \ \eta_2 = 0.30, \ \lambda_1 = 0.00117.$$

Hence, we obtain

$$R_v = 6.4251 > 1.$$

System (3) has an endemic equilibrium,

$$\begin{aligned}
\mathcal{E}_1^{**} &= \left[S_1^{**}, \ S_2^{**}, \ E_1^{**}, \ E_2^{**}, \ V_1^{**}, \ V_2^{**}, \ I_{a,1}^{**}, \ I_{a,2}^{**}, \ I_{s,1}^{**}, \ I_{s,2}^{**}, \ R_1^{**}, \ R_2^{**} \right]^T \\
&= \Big[1.0663e - 01, \ 2.3693e - 02, \ 6.0569e - 04, \ 6.4518e - 06, \\
&\quad 1.6194e - 02, \ 3.0613e - 03, \ 2.0238e - 03, \ 8.2520e - 05, \\
&\quad 5.0185e - 03, \ 5.3556e - 05, \ 1.5170e - 02, \ 2.7128e - 03 \Big]^T.
\end{aligned}$$

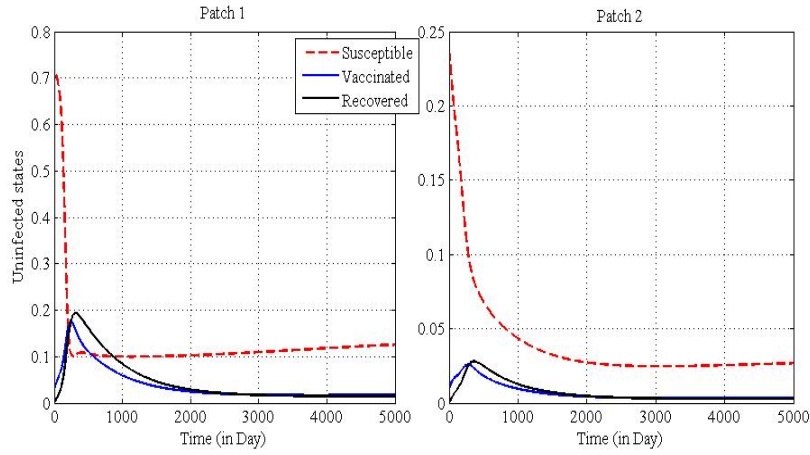Figures 4 and 5 illustrate the stability of $\mathcal{E}_1^{**}$.

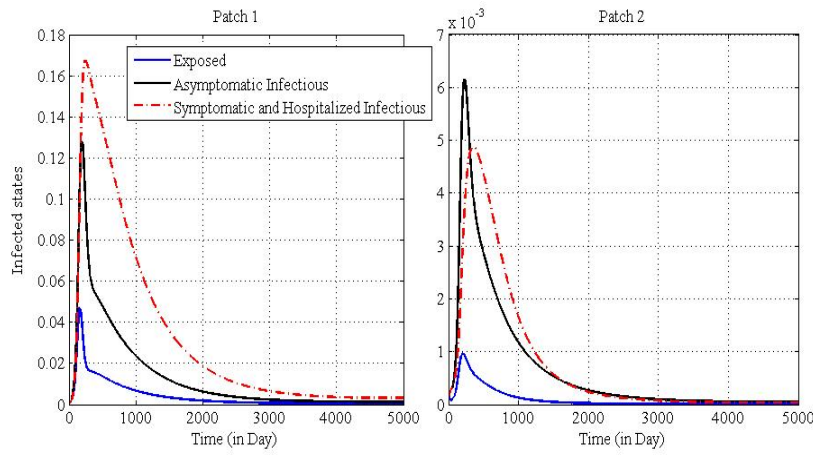Figure 4: Illustration of the stability of $\mathcal{E}_1^{**}$.

Figure 5: Illustrates the stability of $\mathcal{E}_1^{**}$.

By adjusting the key operational parameters to yield varying values of R_v greater than 1, we have

$$R_v = [3.7816,\ 4.6628,\ 5.5440,\ 6.4251,\ 7.3063,\ 8.1875]^T .$$

We observe in Figure 6, the endemic equilibrium point along with standard deviations for each disease state,

$$SD = \Big[3.6400e-02,\ 7.1634e-03,\ 3.8114e-05,\ 4.1860e-07,$$
$$4.1299e-03,\ 8.3947e-04,\ 1.2731e-04,\ 5.2295e-06,$$
$$3.1569e-04,\ 3.4790e-06,\ 3.1924e-03,\ 6.5984e-04\Big]^{T}.$$

These standard deviation values for each disease state indicate that the data points in a set are closely clustered around the mean, suggesting low variability.

Additionally, numerical simulations in Figure 6 show that the solutions with different values of R_v converge to the same endemic equilibrium, where the initial values are

$$S_1\,(0) = 7.1970e-01,\ S_2\,(0) = 2.3990e-01,\ E_1\,(0) = 8.2500e-04,$$
$$E_2\,(0) = 2.7500e-04,\ V_1\,(0) = 2.7975e-02,\ V_2\,(0) = 9.3250e-03,$$
$$I_{a,1}\,(0) = 3.7500e-04,\ I_{a,2}\,(0) = 1.2500e-04,\ I_{s,1}\,(0) = 3.7500e-04,$$
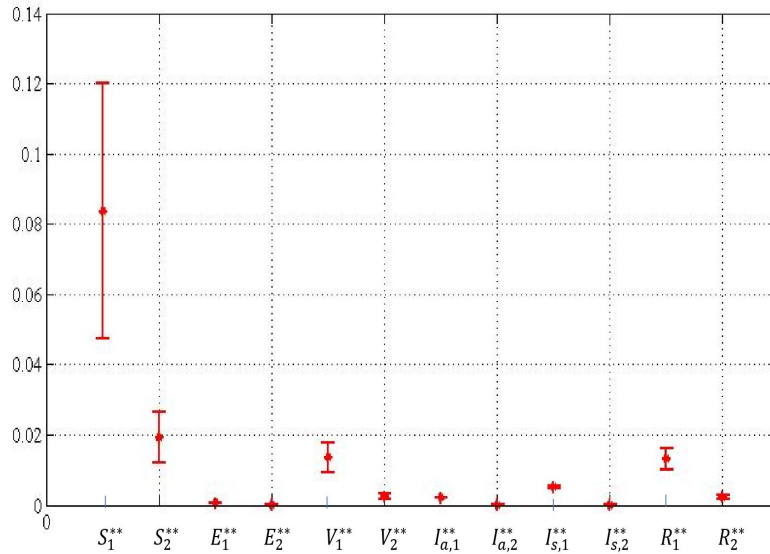$$I_{s,2}\,(0) = 1.2500e-04,\ R_1\,(0) = 4.5000e-04,\ R_2\,(0) = 1.5000e-04.$$

Figure 6: Standard deviation values for each disease state for $\mathcal{E}_1^{**}$.

Certainly, there is a possibility that the endemic equilibrium remains stable given the specified parameters. This leads us to an intriguing question: if the vaccination reproduction number R_v exceeds 1, then the model (3) with migration allows for a locally asymptotically stable endemic equilibrium.

5.4 The effect of migration rate on the transmission of COVID-19 in the two patches

For migration rate values ranging from 0 to 0.01, we observe the results in Figure 7.
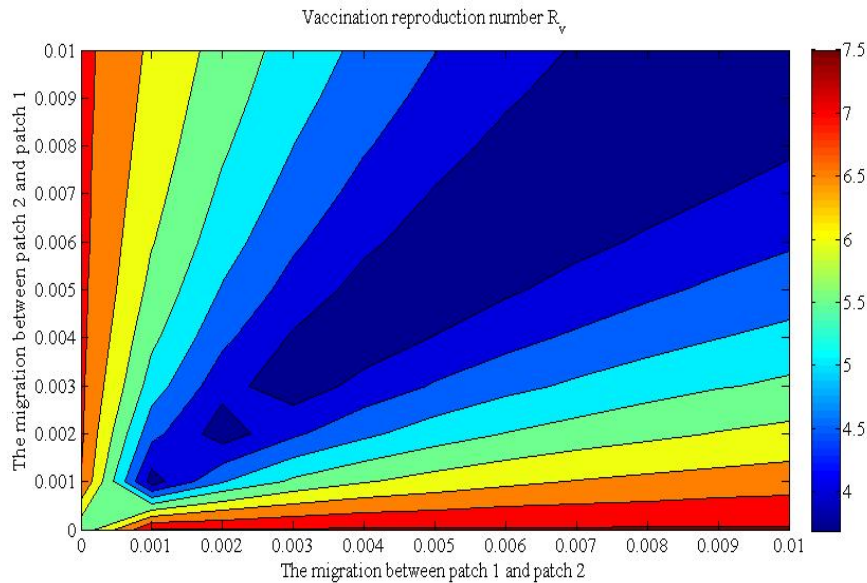

Figure 7: The migration rate effect on R_v.

The numerical simulations presented in Figure 7 underscore the endemic nature of the disease. As the migration rate diminishes from the more populated patch 1 to the less populated patch 2, and concurrently rises from the patch 2 to the patch 1, the vaccine reproduction number Rv demonstrates a proportional increase. This observation validates the outcomes of the sensitivity analysis performed on Rv. Theoretical insights, coupled with these

numerical simulations, emphasize the intricate relationship between COVID-19 prevalence across diverse patches and the corresponding migration rates. These findings contribute to a comprehensive understanding of the dynamics, suggesting that the prevalence is intricately tied to the patterns of migration between distinct patches.

6 Conclusion

In conclusion, the findings from sensitivity analysis shed light on the nuanced interplay between key parameters and the vaccination reproduction number (R_v) in the context of COVID-19 dynamics. Notably, the transmission rate of unconfined individuals (α_2) and the transition rate from exposed to symptomatic infected individuals (β_2) emerge as pivotal factors influencing the increase in R_v. Robust containment measures targeting these aspects, such as stringent protocols, physical barriers, and adherence to social distancing guidelines, are imperative for effective disease control. Furthermore, the vaccination rate (λ_1) and the transition rate from exposed to asymptomatic infected individuals (β_1) closely follow in significance. A 10% increase or decrease in α_2 or β_2 corresponds to substantial changes in R_v, emphasizing the sensitivity of the system. Conversely, a 10% increase in λ_1 or β_1 leads to a notable decrease in R_v. These results provide actionable insights into the impact of parameter variations on the vaccination reproduction number.

For adequate operational data, the stability of DFE $\mathcal{E}_0^*$ suggests the potential for disease eradication. However, elevating the values of sensitive parameters leads to an increase in R_v to 6.4251, surpassing the critical threshold of 1. This instability of $\mathcal{E}_0^*$ indicates the presence of an endemic equilibrium, as per Theorem 2. The theoretical framework aligns with numerical simulations, as depicted in Figures 2 and 3, underscoring the importance of both analytical and computational approaches in understanding the system behavior. The low standard deviation values across different disease states suggest that the data points are closely clustered around the mean, indicating limited variability. Additionally, numerical simulations in Figures 4 and 5 further affirm the endemic nature, demonstrating that varying values of $R_v > 1$ converge to the same endemic equilibrium.

We conclude the simulation by highlighting the complex relationship between COVID-19 prevalence across distinct patches and the corresponding migration rates, offering valuable insights into the dynamic nature of the disease and guiding strategies for effective disease management.

References

[1] Ahmad, R.A., Imron, M.A., Ramadona, A.L., Lathifah, N., Azzahra, F., Widyastuti, K. and Fuad, A. *Modeling social interaction and metapopulation mobility of the COVID-19 pandemic in main cities of highly populated Java Island, Indonesia: An agent-based modeling approach*, Front. Ecol. Evol. 10 (2023), 958651.

[2] Arino, J., Sun, C. and Yang, W. *Revisiting a two-patch SIS model with infection during transport*, Math. Med. Biol. 33(1) (2015), 29–55.

[3] Arino, J. and Van Den Driessche, P. *Disease spread in metapopulations*, Fields Inst. Commun. 48 (2006), 1–12.

[4] Baister, M., McTaggart, E., McMenemy, P., Megiddo, I. and Kleczkowski, A. *COVID-19 in Scottish care homes: A metapopulation model of spread among residents and staff*, medRxiv 2021.08.24.21262524.

[5] Bortolatto, R. *A note on the Lienard-Chipart criterion and roots of some families of polynomials*, arXiv preprint arXiv:1407.4852 (2014).

[6] Boubekeur, M.A. and Belhamiti, O. *Modeling the Impact of Obesity on COVID-19: Evidence from Sensitivity Analysis*, (2023), Submitted.

[7] Bouziane, M., Mezouaghi, A. and Belhamiti, O. *analysis of the vaccination reproduction number and endemic equilibrium to control the Covid-19 spread*, Adv. Math. Sci. App. 32(2) (2023), 399–430.

[8] Castillo-Chavez, C. and Thieme, H. *Autonomous epidemic models*, O. Arino, D. Axelrod, M. Kimmel, M. Langlais (Eds.), Mathematical Population Dynamics: Analysis of Heterogeneity, BU-1248-M (1994) 1–23.

[9] Chen, T.M., Rui, J., Wang, Q.P., Zhao, Z.Y., Cui, J.A. and Yin, L.A. *Model for simulating the phase-based transmissibility of a novel coronavirus*, Infect. Dis. Poverty 9(1) (2020), 1–8.

[10] Chitnis, N., Hyman, J.M. and Cushing, J.M. *Determining important parameters in the spread of malaria through the sensitivity analysis of a mathematical model*, Bull. Math. Biol. 70 (2008), 1272–1296.

[11] Daud, A.A.M. *A note on Lienard-Chipart criteria and its application to epidemic models*, Mathematics and Statistics 9 (2021), 41–45.

[12] Faiçal, N., Ivan, A., Juan, N. and Delfim, T. *Modeling of COVID-19 transmission dynamics with a case study of Wuhan*, Chaos Solit. Fractals. 135 (2020), 109846.

[13] Hancean, M.G., Slavinec, M. and Perc, M. *impact of human mobility networks on the global spread of COVID-19*, J. Complex Netw. 8(6) (2020), 1–14.

[14] Humphries, R., Spillane, M., Mulchrone, K., Wieczorek, S., Riordain, M. and Havel, P. *A metapopulation network model for the spreading of SARS CoV-2: Case study for Ireland*, Infect. Dis. Model. 6 (2021), 420–437.

[15] Iyaniwura, S.A., Ringa, N., Adu, P.A., Mak, S., Janjua, N.Z., Irvine, M.A. and Otterstatter, M. *Understanding the impact of mobility on COVID-19 spread: A hybrid gravity-metapopulation model of COVID-19*, PLoS Comput. Biol. 19(5) (2023), e1011123.

[16] Keddar, M.E.B. and Belhamiti O. *A study of global dynamics and sensitivity analysis of a discrete-time model of the COVID-19 epidemic*, Iranian Journal of Numerical Analysis and Optimization (2023), Accepted. 10.22067/IJNAO.2023.82954.1281

[17] Kim, J.H., SU, W. and Song, Y.J. *On stability of a polynomial*, J. Appl. Math. Inform. 36 (2018), 231–236.

[18] Knobler, S., Mahmoud, A., Lemon, S. and Pray, L. *The impact of globalization on infectious disease emergence and control: Exploring the con-*

sequences and opportunities, Workshop Summary - Forum on Microbial Threats, The National Academies Press, 2006.

[19] Lan Meng, L. and Zhu, W. *SEIR epidemic model for COVID-19 in a multipatch environment, discrete dynamics in nature society*, Discrete Dyn. Nature Soc. 2021 (2021), Article ID 5401253, 1–12.

[20] Martens, P. and Hall, L. *Malaria on the move: human population movement and malaria transmission*, Emerg. Infect. Dis. 6 (2) (2000), 103–109.

[21] McCarthy, C.V., O'Mara, O. and Van Leeuwen, E. *The impact of COVID-19 vaccination in prisons in England and Wales: a metapopulation model*, BMC Public Health, 22 (1003) (2022), 1–17.

[22] Perlman, S., *Another decade, another Coronavirus*, N. Engl. J. Med. 382(8) (2020), 760–762.

[23] Rabitz, H., Kramer, M. and Dacol, D. *Sensitivity analysis in chemical kinetics*, Annu. Rev. Phys. Chem. 34 (1983), 419–461.

[24] Smith, H.L. and Waltman, P. *The theory of the Chemostat*, Cambridge University, 1995.

[25] Van Den Driessche, P. *Reproduction numbers of infectious disease models*, Infect. Dis. Model. 2 (2017), 288–303.

[26] Van Den Driessche, P. and Watmough, J. *Reproduction numbers and sub-threshold endemic equilibria for compartmental models of disease transmission*, Math. Biosci. 180 (2002), 29–48.

[27] Van Den Driessche, P. and Watmough, J. *Reproduction numbers and sub-threshold endemic equilibria for compartmental models of disease transmission*, Math. Biosci 180 (2002), 29–48.

[28] World Health Organization (WHO). *Coronavirus (COVID-19) Dashboard*; (accessed April 17, 2022).

[29] World Health Organization (WHO). *Novel Coronavirus* 2019-nCoV, situation report-1. (accessed May 10, 2021).

[30] Zhao, X. *Systems in population biology*, Springer, 2003.

[31] Zi, Z. *Sensitivity analysis approaches applied to systems biology models*, IET Syst. Biol. 5 (2011), 336–346.